applied sciences

MDPI

Article

Automated Diatom Classification (Part B): A Deep Learning Approach

Anibal Pedraza [1], Gloria Bueno [1,*], Oscar Deniz [1], Gabriel Cristóbal [2], Saúl Blanco [3] and María Borrego-Ramos [3]

[1] VISILAB Research Group, University of Castilla La Mancha, Av. Camilo José Cela s/n, Ciudad Real 13071, Spain; Anibal.Pedraza@uclm.es (A.P.); Oscar.Deniz@uclm.es (O.D.)

[2] Institute of Optics, Spanish National Research Council (CSIC), Serrano 121, Madrid 8006, Spain; gabriel@optica.csic.es

[3] The Institute of the Environment, University of Leon, León E-24071, Spain; Saul.Lanza@unileon.es (S.B.); mborr@unileon.es (M.B.-R.)

* Correspondence: Gloria.Bueno@uclm.es

Academic Editor: Giacomo Cuttone
Received: 8 March 2017; Accepted: 21 April 2017; Published: 2 May 2017

Abstract: Diatoms, a kind of algae microorganisms with several species, are quite useful for water quality determination, one of the hottest topics in applied biology nowadays. At the same time, deep learning and convolutional neural networks (CNN) are becoming an extensively used technique for image classification in a variety of problems. This paper approaches diatom classification with this technique, in order to demonstrate whether it is suitable for solving the classification problem. An extensive dataset was specifically collected (80 types, 100 samples/type) for this study. The dataset covers different illumination conditions and it was computationally augmented to more than 160,000 samples. After that, CNNs were applied over datasets pre-processed with different image processing techniques. An overall accuracy of 99% is obtained for the 80-class problem and different kinds of images (brightfield, normalized). Results were compared to previous presented classification techniques with different number of samples. As far as the authors know, this is the first time that CNNs are applied to diatom classification.

Keywords: convolutional neural networks; deep learning; classification; segmentation; normalization; image acquisition; diatoms

1. Introduction

The specific species found in a water reserve constitute a bioindicator of its quality and whether some kind of activities are more suitable or not. This is stated in international reference documents such as the Directive Framework of Water Policy [1], whose aim is to protect, enhance, and control the quality of rivers, lakes, and seas within the European Union. Scientific evidence shows that biotic indices based on diatoms respond effectively to the presence of elements such as heavy metals, as it is mentioned in [2], and this means that they are quite useful for quality assessment. Diatoms are, together with invertebrates, the most widely used organisms in river quality analysis. Numerous studies also support the effectiveness of biological indices based on diatoms to control the ecological status of water in rivers.

Diatoms have been also studied as paleoenvironmental markers, since their silica structures make it possible to reconstruct the historical environmental conditions by studying the diatom fossil deposits in lake sediments. Therefore, these organisms allow not only to determine the current quality of water reserves but, as [3] suggests, to infer the quality status and environmental variables that dominated in the past. Variations in temperature, pH or conductivity over centuries can be estimated by studying these organisms in sediments, allowing not only to know how climate has affected the studied area, but to state the baseline conditions from which we can set criteria for optimal quality for a water reserve, according to [1].

The application of the most widespread diatom indices often requires a precise level of classification, which involves time and expert training. Moreover, the identification of morphological microstructures and frustule (the series of linking, siliceous bands associated with a valve) discrimination from other elements in the image (fractionated cells or mineral particles) is still unresolved. Some diatoms that were considered the same species for decades, have been now separated into different species and, moreover, the emergence of new species is continuous. The development of tools for automatic diatoms identification and classification that take into account the contour as well as texture information would be helpful in a wide range of applications for both experts and non-experts. However, automatic diatom classification is still an open challenge.

Some works have been reported in the literature to automatically classify diatoms. However, they have been based on general state-of-art features, which are limited and maybe not suitable enough for this problem. Moreover, the developed models are only valid for a limited subset of species. Hence, the number of analyzed species has been limited and the results are relatively poor, decreasing the performance when increasing the number of species. The proposed method relies on a technique that builds specific features regarding the input that is provided, keeping the performance when the number of species that are studied grows. The only drawback is the huge amount of data that is necessary to perform the training process, but in this case there is enough available.

The best results so far have been presented by the authors in the previous study [4], where 98.1% accuracy is reported for the classification of 80 species with a total of 24,000 segmented samples. Another large dataset with 55 species but with lower number of samples (1093) was presented by Dimitrovski et al. [5] with a result of 96.17%. This result improved to 97.97% with less classes (38 diatom types) and 837 samples in total.

Regarding the application of deep learning, the difficulty is to build a model able to distinguish among thousands of classes, with an average of 700 image samples per class. Most of the improvements in Convolutional Neural Network (CNN) models, such as inception modules, are aimed at improving accuracy results. Models such as *AlexNet* ([6], winner in ImageNet Large Scale Visual Recognition Competition (ILSVRC) 2010 and 2012) and *GoogLeNet* ([7], winner in ILSVRC 2014) have achieved impressive results in the past and have become state of art models for this reason.

To summarize, different classification techniques using different features have been presented in the literature to classify diatom types, ranging between 14 to 80 species, with databases not larger than 30,000 samples. The maximum overall accuracy obtained is 98.1%. Table 1 presents a summary of these works together with the proposed one. Table 1 shows the number of diatom types (Num. Species), the total number of samples (Num. Samples), the classification method and the results.

Table 1. Related work and results summary.

Year [Reference]	Num. Species	Num. Samples	Num. of Features and Type	Classifier	Accuracy (%)
2002 [8]	37	781	321 from Geometrical, Textural, Morphological and Frequency	Bagging Tree	96.9
2003 [9]	1	66	10 Morphological	Multiple Discriminant Analysis	80.3
2012 [5]	38	837	30 Morphological and 200 Texture	Random forest	97.97
	48	1019	30 Morphological and 200 Texture	Random forest	97.15
	55	1098	30 Morphological and 200 Texture	Random forest	96.17
2016 [10]	14	10,000	4 Geometrical 7 Moments and 33 Morphological	SVM	94.7
2017 [4]	80	24,000	273 Morphological, Statistical, Textural, Space-Frecuency	Bagging Tree	98.1
Proposed	80	24,000	CNN-AlexNet	Softmax	95.62
Proposed	80	160,000	CNN-AlexNet	Softmax	99.51

In this study, we do a deep analysis of CNN techniques with a significant database composed of a maximum of 160,000 brightfield samples. The raw data is composed by nearly 11,000 diatom samples labeled by the expert. After the image processing workflow and the first iteration of the data augmentation, 69,350 samples are available. Further iterations of the data augmentation process are performed, using rotations of 2°, to obtained the number of samples stated before. Additional datasets have been built applying some common preprocessing techniques such as segmentation or normalization over the raw data. These datasets are described in Section 2. In Section 3 the deep learning approach is described and the results are shown in Section 4, the performance ranges between 95.62% to 98.81%. For the first accuracy, we used a segmented database composed of 300 samples, the same database used in the previous study (previous article [4]). The better accuracy is obtained with an augmented version of the dataset, only applied in this method, since [4] states that the accuracy in traditional methods do not improve with augmented data (it is also counterproductive due to orientation-invariant features and overfitting). Using augmented and combined datasets results improve up to 99.51%. There, a dataset composed by non-treated and normalized images, limited to 2000 samples per species is used. Finally, conclusions are presented in Section 5.

2. Materials

This section is focused on the process carried out to create a dataset of diatom species that are representatives of the problem, applying CNNs after that to perform classification. In order to perform the first task, the collaboration of an expert diatomist was needed. In our work, the co-authors Dr. Saúl Blanco and María Borrego-Ramos were the responsible of this process.

The main stages necessary to create a dataset of this kind are: species selection, image acquisition, data labeling, image processing, data augmentation, and finally, the dataset building itself. The species selection and image acquisition is equal to the one described by the authors in the previous paper [4]. Here we will describe the other stages.

2.1. Data Labeling

Once the species have been selected and the images digitized, several images were obtained. However, they can be considered as "raw data" since there is a lack of information about what kind of specimens can be found or where they are located. To use these images for training, a process of labeling must be accomplished. This task consists of manually selecting where the diatoms are, indicating to which class they belong. To facilitate the process, a labeling tool was provided to the expert.

2.2. Image Processing

The next step is to use the information produced at the labeling step, so that every single specimen and its information can be cropped from the original pictures. These samples had a small size (around 120×120 pixels) and, as it will be detailed next, will conform the basis for the main dataset that will be completed.

One substep has to be mentioned here. Due to mislabeling from the biologist, there were some samples that did not meet the requested quality parameters. If this data was piped to the rest of the workflow, noise would be introduced in the dataset. For this reason, a manual check over the selected Regions Of Interest (ROIs) by the expert is needed, so the actual amount of samples reduced slightly at this point, with an average drop rate of 25%.

2.3. Data Augmentation

A suitable ratio must be maintained between the number of classes and the number of samples per class, since it has a great impact on learning. To overcome this, there are some techniques that artificially increase the number of available data without obtaining new samples (the latter is not suitable due to the reasons previously mentioned). In computer vision, this process is known as Data Augmentation.

In this process, rotation and flips were applied: rotation by 0°, 90°, 180°, 270° and flip for each one. This increased the amount of training data by a factor of eight.

2.4. Dataset Building

After this process, a primary dataset is available, with 69,350 samples of the 80 species. The list of species and the number of samples are detailed in Table 2. Since this data is not enough to further develop experiments with 300, 700, 1000 and 2000 balanced samples per class, extra iterations of the data augmentation stage are performed, using 2° degrees rotations until the necessary amount of samples are obtained. This way, new datasets with the necessary number of samples per class can be obtained for these experiments, just by limiting the images that are taken: from 24,000 (80×300), 56,000 (80×700), 80,000 (80×1000) to 160,000 (80×2000).

Table 2. Diatom species chart, showing the total number of samples per class.

1. *Achnanthes subhudsonis*	984	2. *Achnanthidium atomoides*	1032
3. *Achnanthidium caravelense*	472	4. *Achnanthidium catenatum*	1496
5. *Achnanthidium druartii*	744	6. *Achnanthidium eutrophilum*	776
7. *Achnanthidium exile*	784	8. *Achnanthidium jackii*	1000
9. *Achnanthidium rivulare*	2440	10. *Amphora pediculus*	936
11. *Aulacoseira subarctica*	904	12. *Cocconeis lineata*	648
13. *Cocconeis pediculus*	392	14. *Cocconeis placentula var euglypta*	936
15. *Craticula accomoda*	688	16. *Cyclostephanos dubius*	680
17. *Cyclotella atomus*	792	18. *Cyclotella meneghiniana*	824
19. *Cymbella excisa var angusta*	632	20. *Cymbella excisa var excisa*	1928
21. *Cymbella excisiformis var excisiformis*	1136	22. *Cymbella parva*	1416
23. *Denticula tenuis*	1448	24. *Diatoma mesodon*	920
25. *Diatoma moniliformis*	1072	26. *Diatoma vulgaris*	704
27. *Discostella pseudostelligera*	656	28. *Encyonema minutum*	960
29. *Encyonema reichardtii*	1216	30. *Encyonema silesiacum*	864
31. *Encyonema ventricosum*	808	32. *Encyonopsis alpina*	848
33. *Encyonopsis minuta*	712	34. *Eolimna minima*	1392
35. *Eolimna rhombelliptica*	1056	36. *Eolimna subminuscula*	752
37. *Epithemia adnata*	576	38. *Epithemia sorex*	680
39. *Epithemia turgida*	744	40. *Fragilaria arcus*	744
41. *Fragilaria gracilis*	432	42. *Fragilaria pararumpens*	592
43. *Fragilaria perminuta*	712	44. *Fragilaria rumpens*	392
45. *Fragilaria vaucheriae*	656	46. *Gomphonema angustatum*	688
47. *Gomphonema angustivalva*	440	48. *Gomphonema insigniforme*	720
49. *Gomphonema micropumilum*	712	50. *Gomphonema micropus*	936
51. *Gomphonema minusculum*	1264	52. *Gomphonema minutum*	744
53. *Gomphonema parvulum f saprophilum*	416	54. *Gomphonema pumilum var elegans*	1024
55. *Gomphonema rhombicum*	512	56. *Humidophila contenta*	840
57. *Karayevia clevei var clevei*	672	58. *Luticola goeppertiana*	1088
59. *Mayamaea permitis*	320	60. *Melosira varians*	1168
61. *Navicula cryptotenella*	1088	62. *Navicula cryptotenelloides*	856
63. *Navicula gregaria*	400	64. *Navicula lanceolata*	616
65. *Navicula tripunctata*	792	66. *Nitzschia amphibia*	992
67. *Nitzschia capitellata*	984	68. *Nitzschia costei*	576
69. *Nitzschia desertorum*	568	70. *Nitzschia dissipata var media*	648
71. *Nitzschia fossilis*	608	72. *Nitzschia frustulum var frustulum*	1808
73. *Nitzschia inconspicua*	2040	74. *Nitzschia tropica*	520
75. *Nitzschia umbonata*	728	76. *Rhoicosphenia abbreviata*	752
77. *Skeletonema potamos*	1240	78. *Staurosira binodis*	752
79. *Staurosira venter*	696	80. *Thalassiosira pseudonana*	560

This original dataset contains sample images without applying any kind of processing, i.e., the diatoms as acquired by the expert. Figure 1 shows a mosaic with one image sample per species.

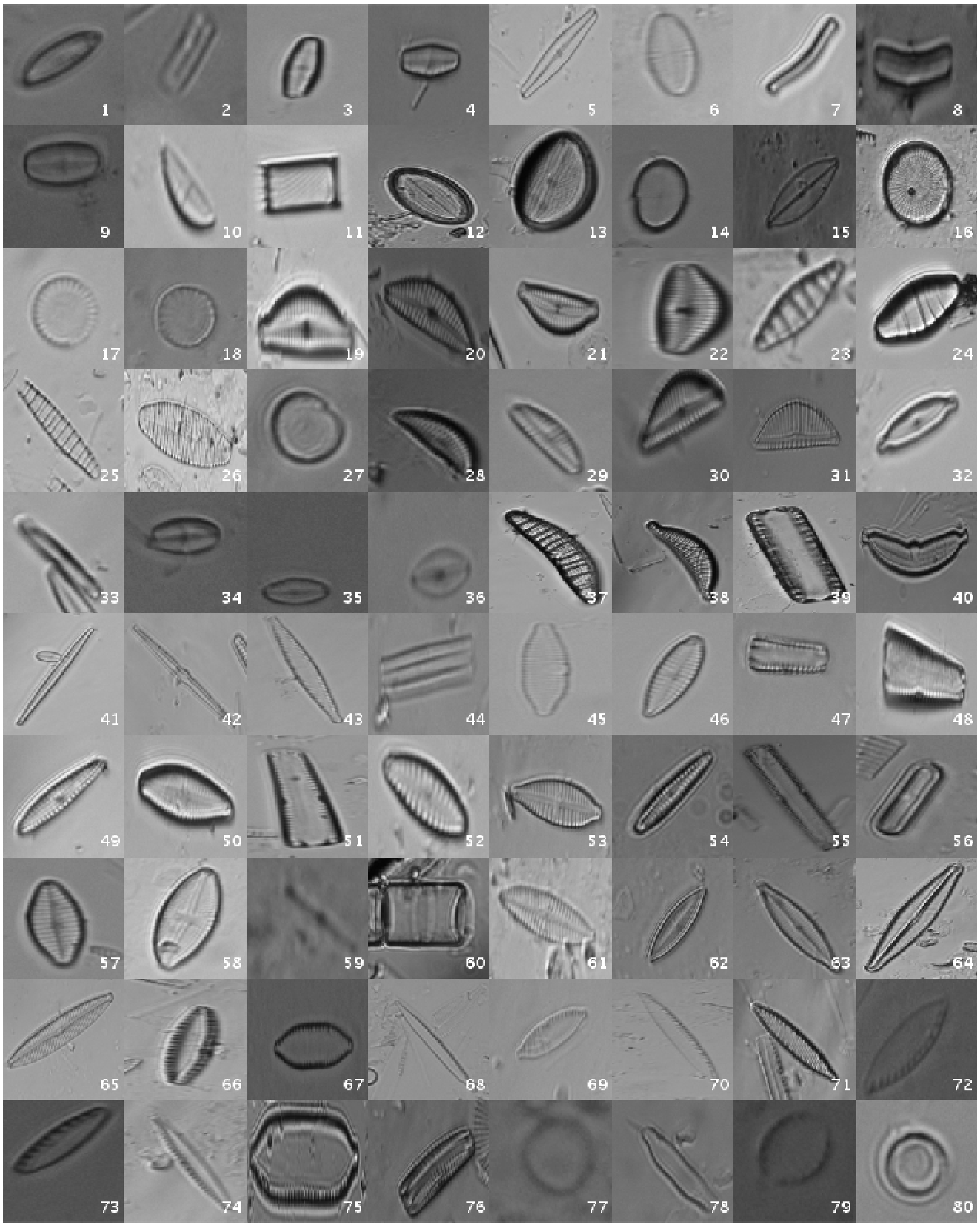

Figure 1. Examples of diatom classes in the original dataset.

In order to study the influence of image contrast, background, histograms and heterogeneity, some additional datasets have been built from this original one, applying different image processing techniques.

2.4.1. Segmented Dataset

One of the traditional image processing techniques that is usually applied is segmentation, in which only the interesting object in the image is conserved, turning the rest of it into black, applying some kind of mask. The exact method that was used to develop this dataset is described in the previous article from this issue [4]. In summary, the segmentation is done by means of a binary thresholding where the segmented region are binary masks where descriptors must be computed.

The process to obtain the binary masks consists of four steps:

1. *Binary Thresholding*: automatic segmentation based on Otsu's thresholding.
2. *Maximum area*: calculation of the largest region (area).
3. *Hole filling*: interior holes are filled if present.
4. *Segmentation*: the ROI is cropped with the coordinates of the bounding-box of the largest area (step 2).

Figure 2 shows a mosaic with one image sample per species.

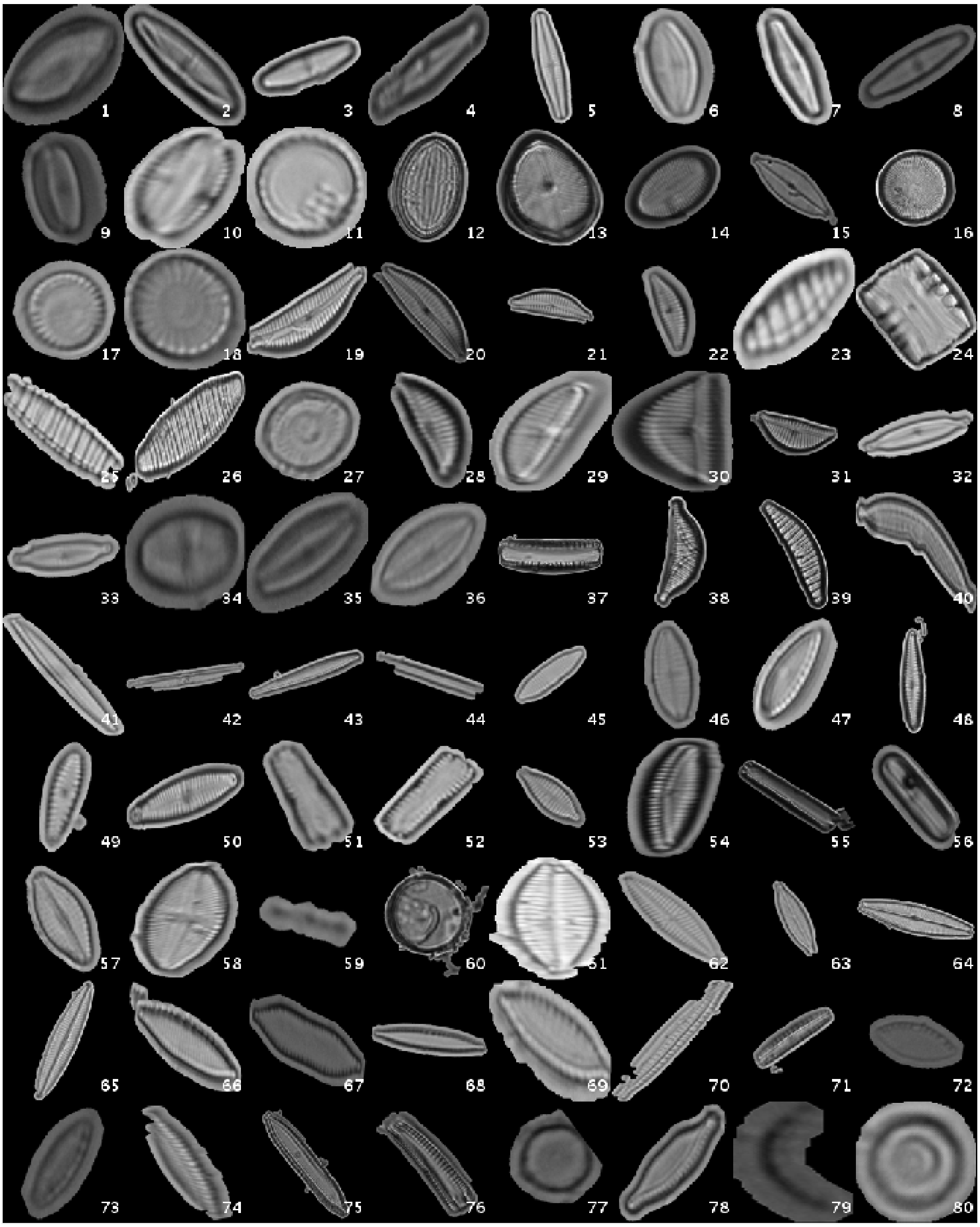

Figure 2. Diatom classes examples for segmented dataset.

2.4.2. Normalized Dataset

In order to study whether different image contrast and illumination conditions among the species may affect learnings and discriminations, a global normalization is applied to obtain a new dataset. The technique that has been employed is histogram matching, described in [11]. The fundamental of this process is to select a reference image, with good contrast and definition, and fit the histogram of the rest of images to that one.

The technique follows this process: the histograms of the reference R and target T images are computed. After that, the cumulative distribution functions (F) of those histograms are calculated. Using that information, the goal is to determine which grey level ($G_{0.255}$) in the target image fulfills that ($F_R(G_i) = F_T(G_i)$). This is applied to every single pixel in target images.

Figure 3 shows a mosaic with one image sample per species.

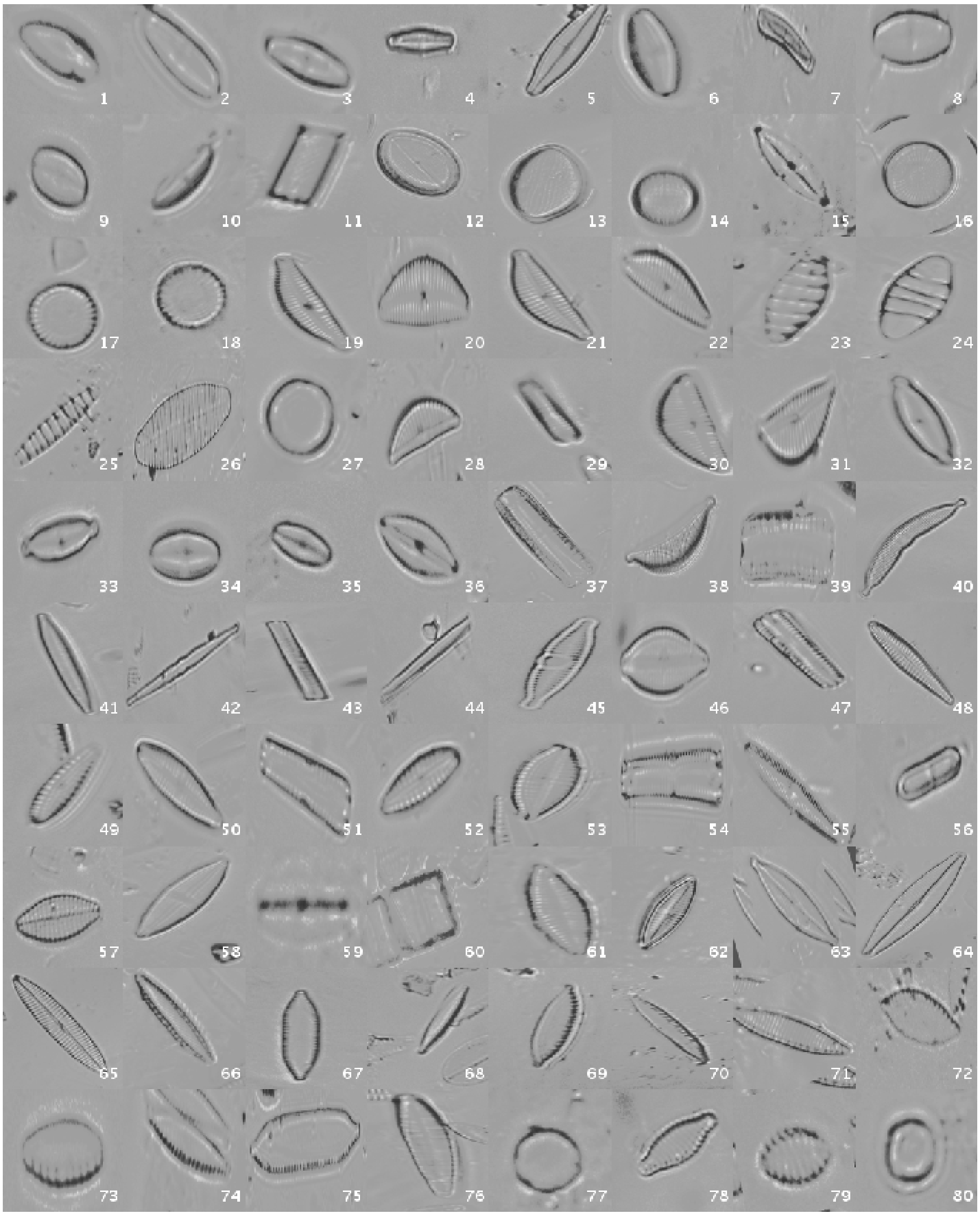

Figure 3. Diatom examples in the normalized dataset.

2.4.3. Original + Normalized Dataset

Finally, an heterogenous dataset is built. In this case, the images from original and normalized datasets are merged, so that this dataset would be useful to study whether the variety of image sources and features contributes to the accuracy in the classification process.

3. Deep Learning

The approach is based on applying the CNN paradigm to the different datasets that have been generated. First of all, a general overview is provided. After that, the specific details about training, testing and validation processes are explained.

3.1. Convolutional Neural Networks

CNNs are based on simple neural networks, with some additional features. These are mainly new ways of organizing and applying the neurons to the data. Numerical parameters rule the learning process and its tuning can be crucial to obtain good results.

The network is fed with every single sample and the answer the net provides is improved applying several iterations, making it closer to the expected answer minimizing the loss function. The exact mathematical mechanisms to solve this problem are the so-called *solvers*. Among them, Stochastic Gradient Descent (SGD), is the basis and the most common, but there also are important variants like Adaptive Gradient (AdaGrad) presented in [12] or Nesterov Accelerated Gradient (NAG) introduced in [13].

3.2. Training

The method that has been developed takes advantage of a transfer learning technique called fine-tuning. That is, taking a previously trained model that has learned good general features and apply that to our own dataset, adapting the network weights for the problem at hand. The model used was a pretrained AlexNet model from the ImageNet challenge (see [6]). Given that, it was possible to achieve good results with only a few epochs/iterations. Figure 4 shows how this network is organized, an input image is provided and, after the neuronal activations throughout the layers, a percentage of confidence in the decision class is provided. In Table 3, the architecture layers are presented in detail.

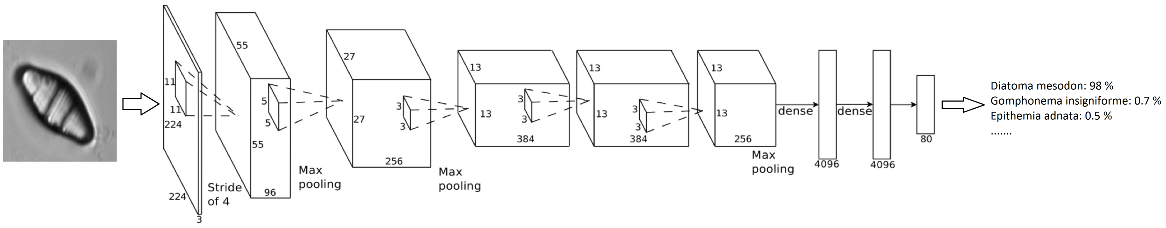

Figure 4. AlexNet Network architecture.

The training process is started out with an initial learning rate of 0.001, decreasing it with a drop factor of 0.1 with a period of 8. For back propagation, the Stochastic Gradient Descent was used, establishing 0.004 for L2-Regularization. With the previous parameters, training reaches the best results with just 10 epochs (after that number the loss value and accuracy do not improve). It takes around 1 h to perform a training process (i.e., training one fold of cross-validation), using the GPU NVIDIA GTX 960 Ti with 6 GB of VRAM. To perform the experiments, 10 fold cross-validation has been applied, with 9 folds for training and the remaining one in each iteration for testing.

As described in the publication of the architecture that is employed in this work ([6]), there are two techniques that this method applies to face overfitting, one of the major problems of Deep Learning. The first one is data-augmentation, since the application of rotations and reflections over the input images ensures that different versions of the same samples are provided, so that the features the model learns are more general. The other one is the use of dropout layers in the architectures (which are present in the model that is employed). The idea is to randomly "turn off" some of the neurons, so local dependencies throughout the network are avoided, making the model more robust.

Table 3. AlexNet architecture layers.

Layer Type	Size	Number of Kernels	Number of Neurons
Image input	224×224×3		150,528
Convolution	11×11×3	96	253,440
ReLU			
Channel normalization			
Pooling			
Convolution	5×5×48	256	186,624
ReLU			
Channel normalization			
Pooling			
Convolution	3×3×256	384	64,896
ReLU			
Convolution	3×3×192	384	64,896
ReLU			
Convolution	3×3×192	256	43,264
ReLU			
Pooling			
Fully connected			4096
ReLU			
Dropout			
Fully connected			4096
ReLU			
Dropout			
Fully connected			80
Softmax			
Classification			

3.3. Testing

Taking the 10% of the dataset that was reserved for testing in each fold, the trained model was applied to these images, classifying each one individually and calculating the resulting confusion matrix. Using the hardware described above, it takes around 0.007 s to classify a single image.

3.4. Validation

Once any image analysis method has been applied, it is important to quantify the performance to know how accurate it is or compare it with other methods. The most widely used technique to measure the behavior of a classifier is the *Confusion Matrix*. T. Fawcett performs a comprehensive review of this topic in [14]. Here, the most important concepts are summarized.

The *Confusion Matrix* is a tabular representation which states the relationship between the predicted instances and the correct results. This way, there are four kinds of items:

- *True Positive.* The instance belongs to the class and so is predicted.
- *False Positive.* The instance does not belong to the class but is predicted as positive. This is the so-called *Type I error*.
- *True Negative.* The instance does not belong to the class and so is predicted.
- *False Negative.* The instance does belong to the class but is predicted as negative. This is the so-called *Type II error*.

From this matrix, some metrics can be calculated to summarize the performance in certain aspects. The most important ones are:

- True Positive Rate (TPR) or Sensitivity. Defined in Equation (1), it measures the proportion of positive samples correctly classified.

$$\frac{\sum True\ positive}{\sum True\ positive + \sum False\ negative} \tag{1}$$

- True Negative Rate (TNR) or Specificity. Defined in Equation (2), it measures the proportion of negative samples correctly classified.

$$\frac{\sum True\ negative}{\sum False\ positive + \sum True\ negative} \tag{2}$$

- Accuracy. Defined in Equation (3), it measures the proportion of correctly classified samples (positives and negatives) against the total population (number of samples that have been classified).

$$\frac{\sum True\ positive + \sum True\ negative}{\sum Total\ population} \tag{3}$$

4. Results and Discussion

Using the datasets and the method introduced in the previous section, some experiments have been performed, varying the number of samples for training and applying cross-validation to check the performance of convolutional neural networks in this problem. Hence, the training is based on using the same number of samples per species throughout the 80 classes, so the experiments are balanced. The decision is to set those values at 300, 700 and 1000 samples per species. When more samples were needed, some extra rotation with fewer degrees step gap (typically 2°) were applied.

The results are illustrated using a heat map representation of the confusion matrices. The colorbar means the percentage of images (between 0 and 1) from a given class (row) that has been classified as the species in the corresponding column.

4.1. Original Dataset

The confusion matrices for training with 300, 700 and 1000 samples per class are presented in Figures 5–7 respectively.

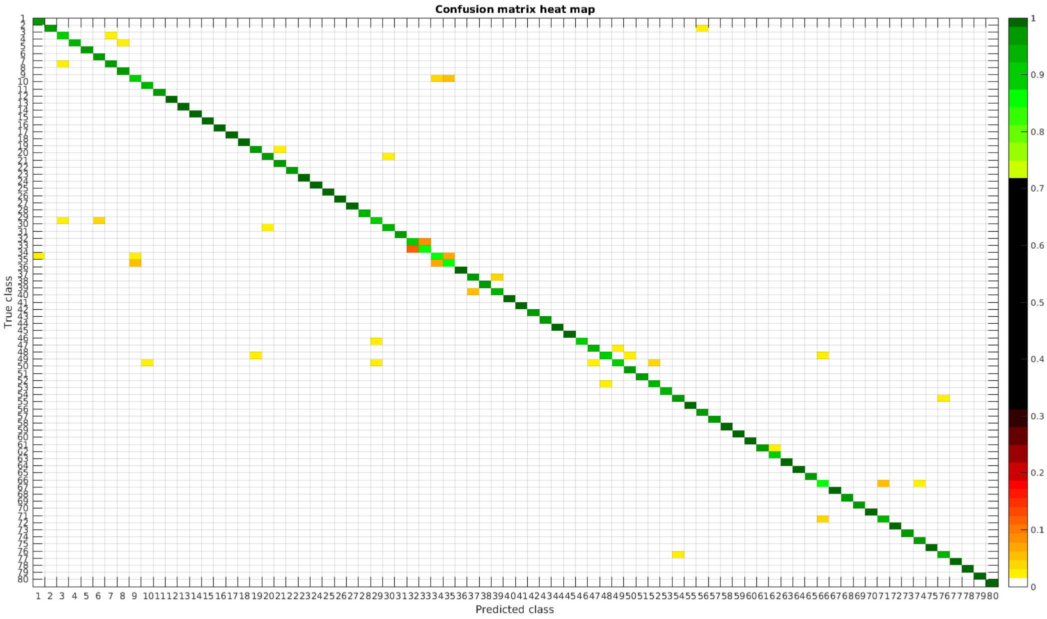

Figure 5. Confusion matrix heat map for the original dataset with 300 samples per class.

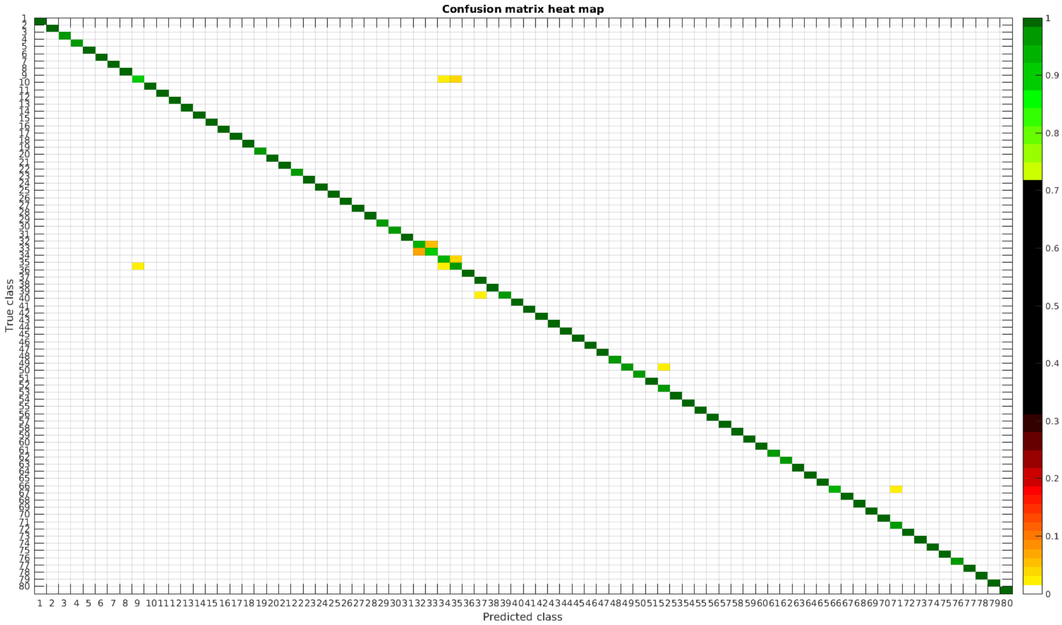

Figure 6. Confusion matrix heat map for the original dataset with 700 samples per class.

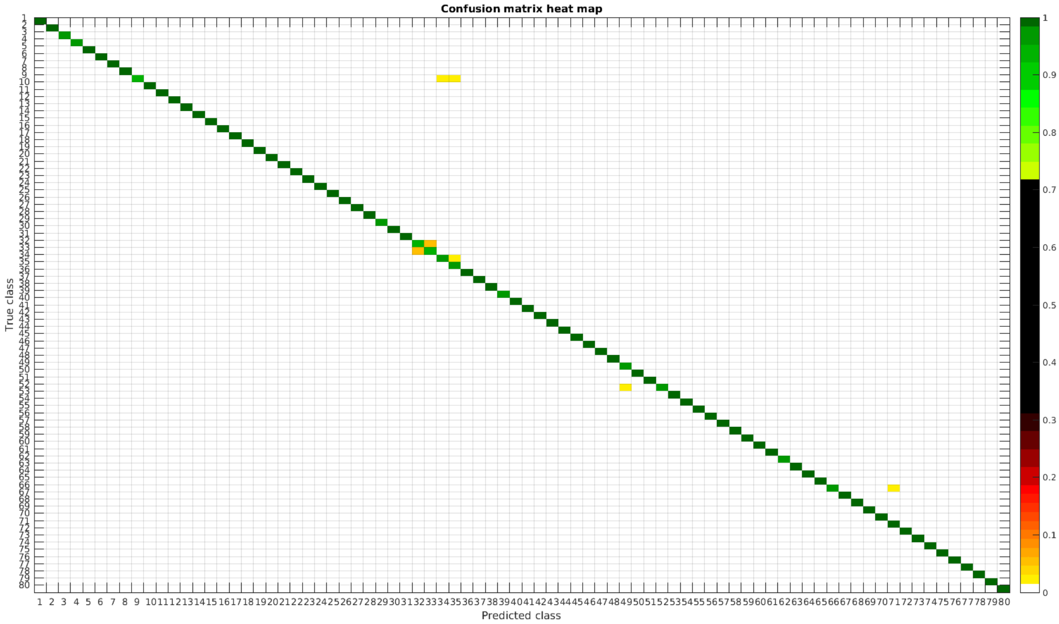

Figure 7. Confusion matrix heat map for the original dataset with 1000 samples per class.

Table 4 shows a summary of experiments with the original database, giving precise information about the dataset, the number of samples per class, the mean accuracy of the 10 folds from cross-validation and standard deviation. The accuracy for testing has been calculated as the percentage of labels that match between the ground truth and the classifier. Notice that when the number of samples per species is increased, the accuracy is improved and only some of the confusions remain.

In Figure 8, a summary of the most frequent confusions is shown, where, the first row shows a confusion between *Achnanthidium caravelense* (3) and *Achnanthidium exile* (7). Further than belonging to the same family, the confusion is most likely to be produced because of the presence of “valve view” (the view of the frustule when the valve is uppermost) and “girdle view” (the view of the frustule when the girdle is uppermost) samples in the dataset, the latter being much more difficult to be distinguished from each other. A similar appearance of the images would be the most common source of confusions throughout the different experiments.

The diatom species that show initially a larger error are: *Encyonopsis alpina* (32), *Encyonopsis minuta* (33), *Eolimna minima* (34) and *Eolimna rhombelliptica* (35).

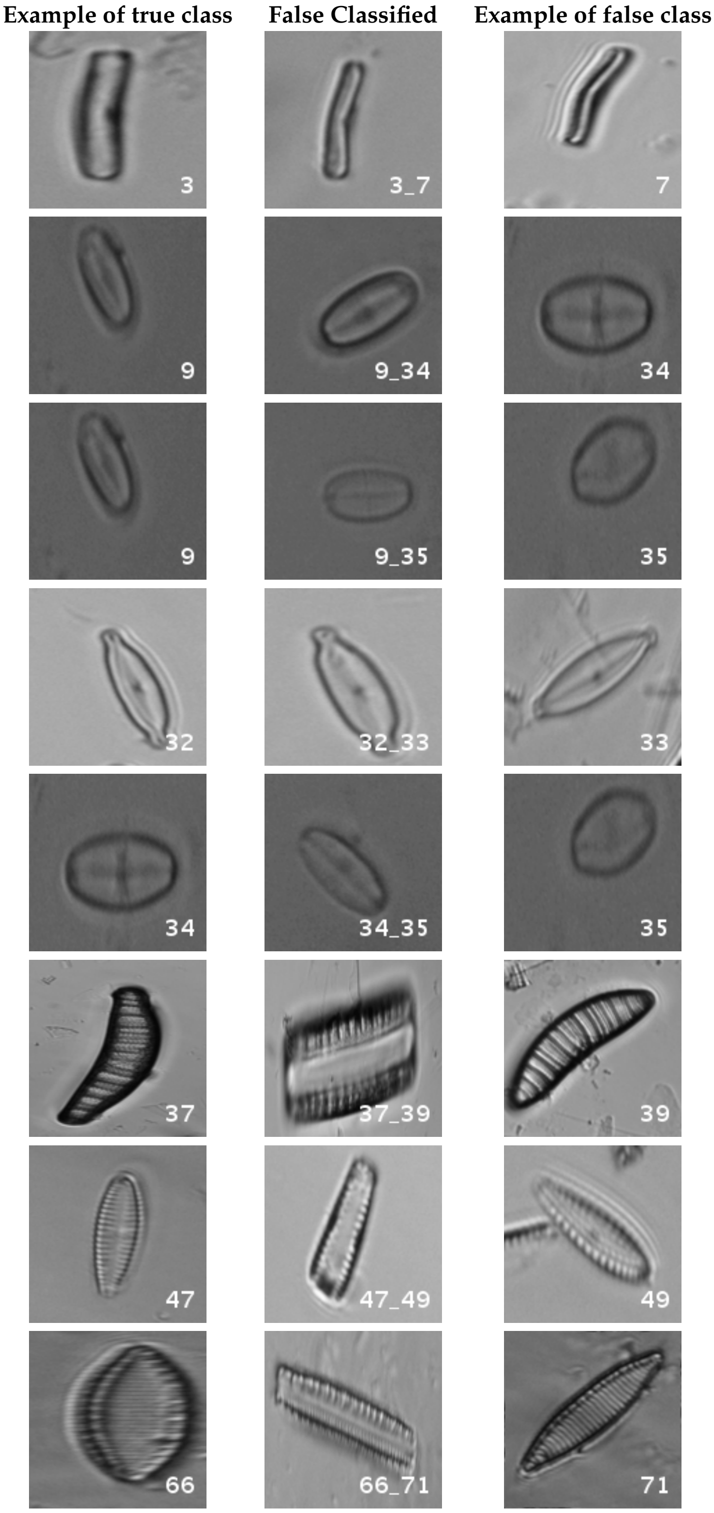

Figure 8. Original dataset main confusions. Each row shows an example of the true species, a missclassified sample between two species and a sample of the second one are shown.

Table 4. Deep Learning experiments with the original database.

Dataset	Samples per Class	Mean Accuracy (%)	Standard Deviation
Original	300	96.35	0.44
Original	700	98.64	0.13
Original	1000	99.24	0.09

4.2. Segmented Dataset

Using the segmented dataset, the same experiments were performed. The confusion matrices for training with 300, 700 and 1000 samples per class are presented in Figures 9–11, respectively.

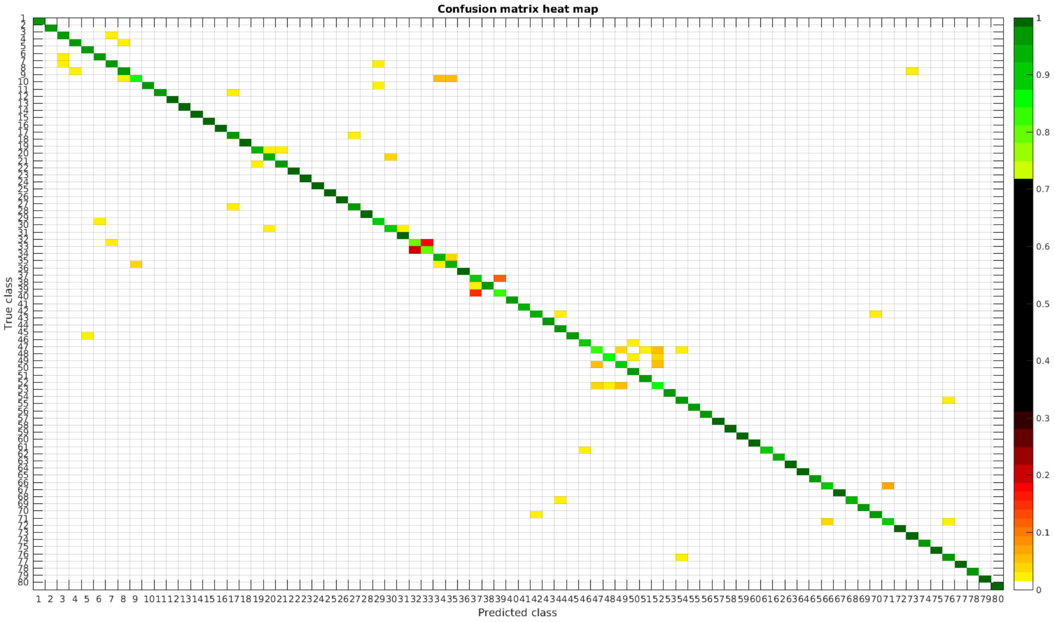

Figure 9. Confusion matrix heat map for the segmented dataset with 300 samples per class.

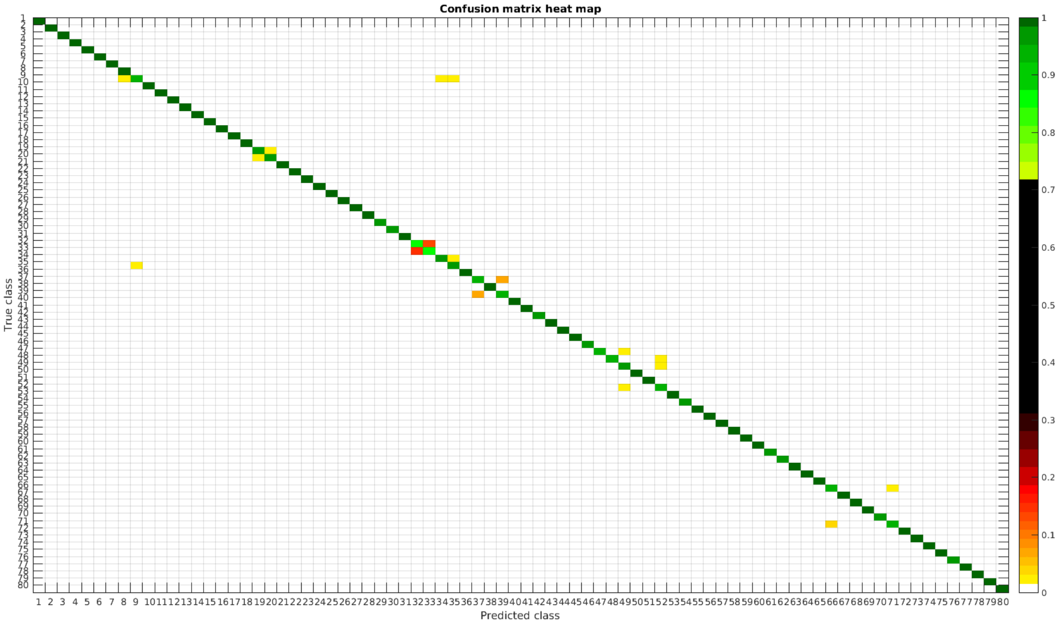

Figure 10. Confusion matrix heat map for the segmented dataset with 700 samples per class.

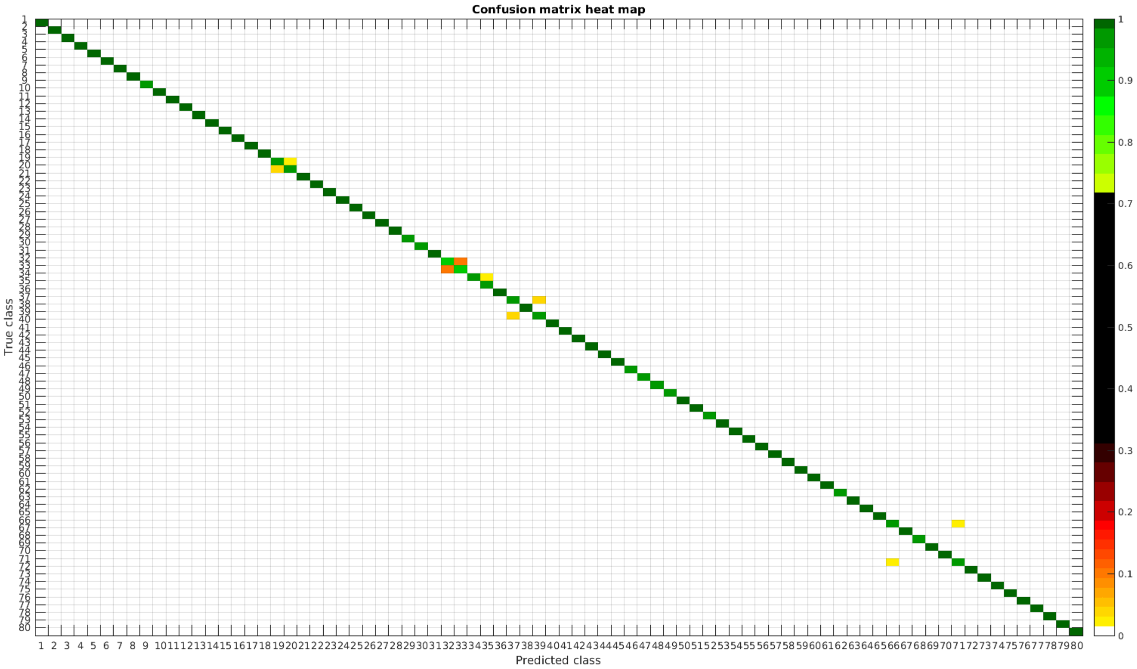

Figure 11. Confusion matrix heat map for the segmented dataset with 1000 samples per class.

In Figure 12, a summary of the most frequent confusions is shown.

In this dataset, again, the majority of bad classifications are due to species that are quite similar to each other. However, in comparison with the previous dataset, there are more pairs of species that maintain a (relatively) significant error rate. These are:

- *Cymbella excisa var angusta* (19) and *Cymbella excisa var excisa* (20);
- *Encyonopsis alpina* (32) and *Encyonopsis minuta* (33)—same than the original database;
- *Eolimna minima* (34) and *Eolimna rhombelliptica* (35) —same than the original database;
- *Epithemia adnata* (37) and *Epithemia turgida* (39);
- *Nitzschia amphibia* (66) and *Nitzschia fossilis* (71).

Once again as the number of training samples per species is increased, the accuracy improves, and most of the confusions disappear. Table 5 shows a summary of the experiments with the segmented database. Notice that this database is the same that the one used in the previous article [4]. The handcrafted approach based on bagging tree performs better for lower number of samples, that is for 300 samples per class the overall accuracy was 98.11% versus the current 95.62% with CNN. The result, as compared with classical handcrafted approaches only improves when the database is larger than 700 samples per class.

Table 5. Deep Learning experiments with the segmented database.

Dataset	Samples per Class	Mean Accuracy (%)	Standard Deviation
Segmented	300	95.62	0.48
Segmented	700	98.27	0.15
Segmented	1000	98.81	0.15

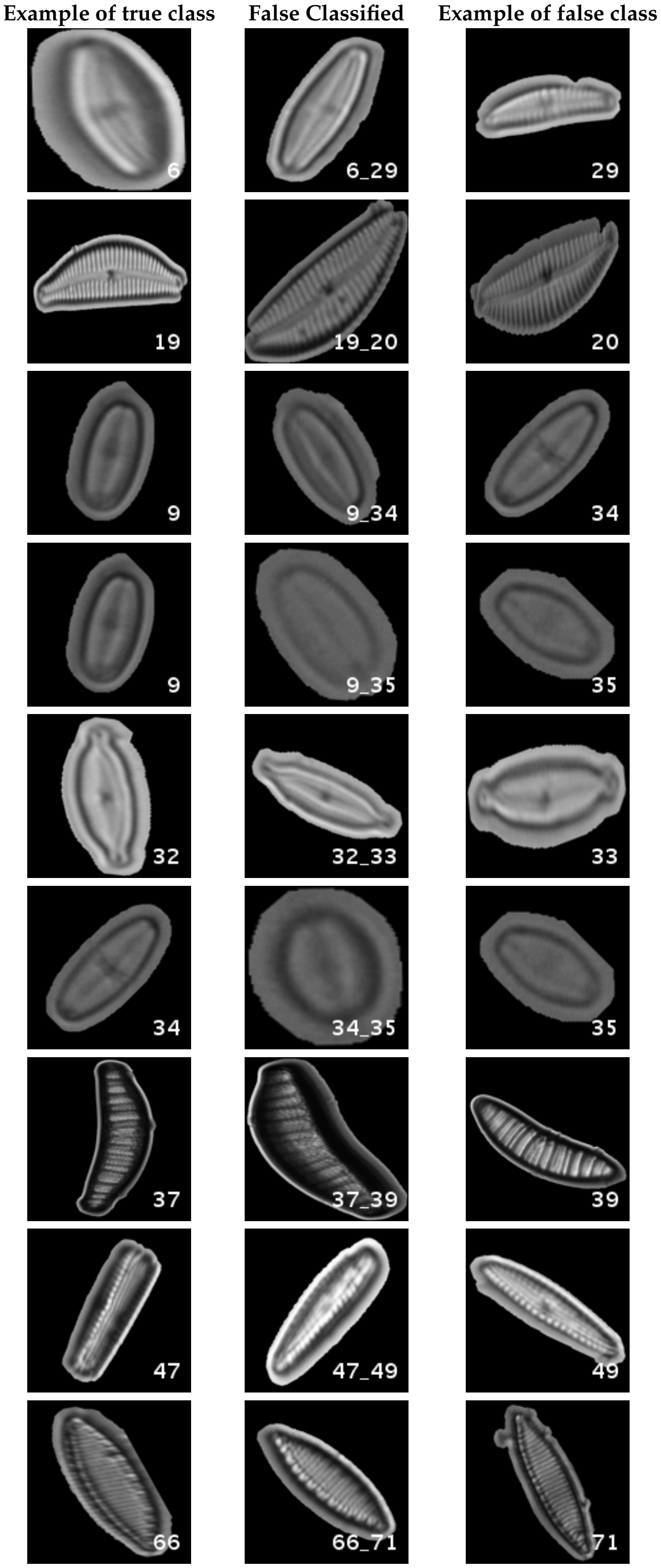

Figure 12. Segmented dataset main confusions. Each row shows an example of the true species, a missclassifed sample between two species and a sample of the second one are shown.

4.3. Normalized Dataset

The confusion matrices for training with 300, 700 and 1000 samples per class are presented in Figures 13–15, respectively.

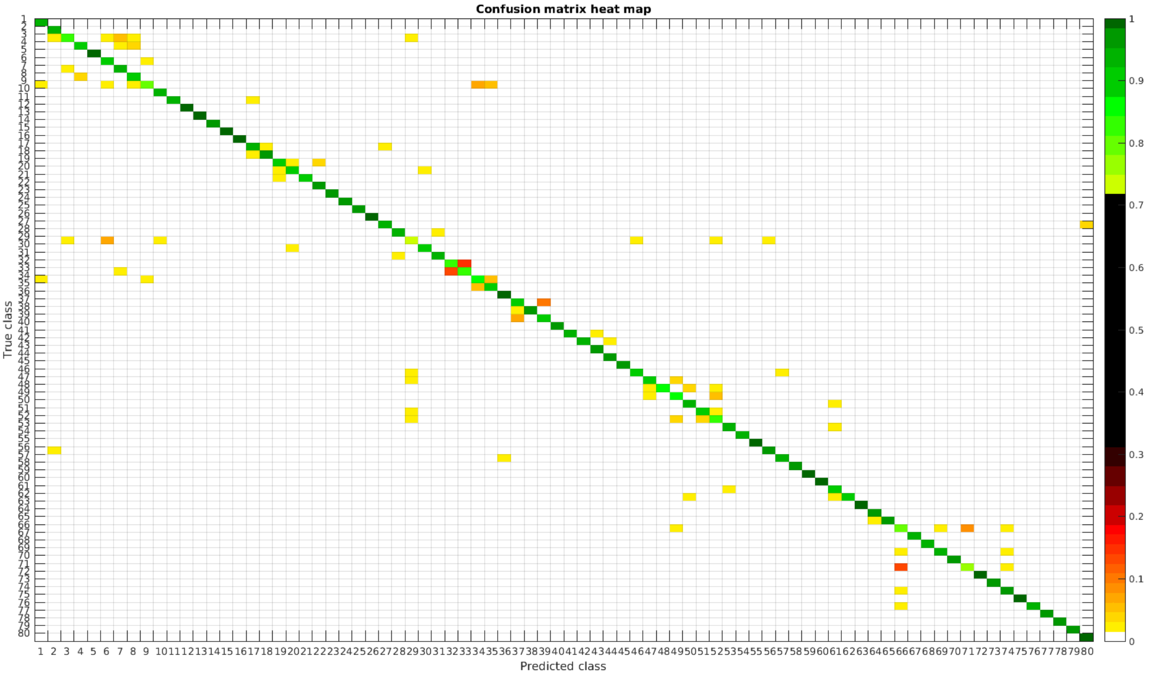

Figure 13. Confusion matrix heat map for the normalized dataset with 300 samples per class.

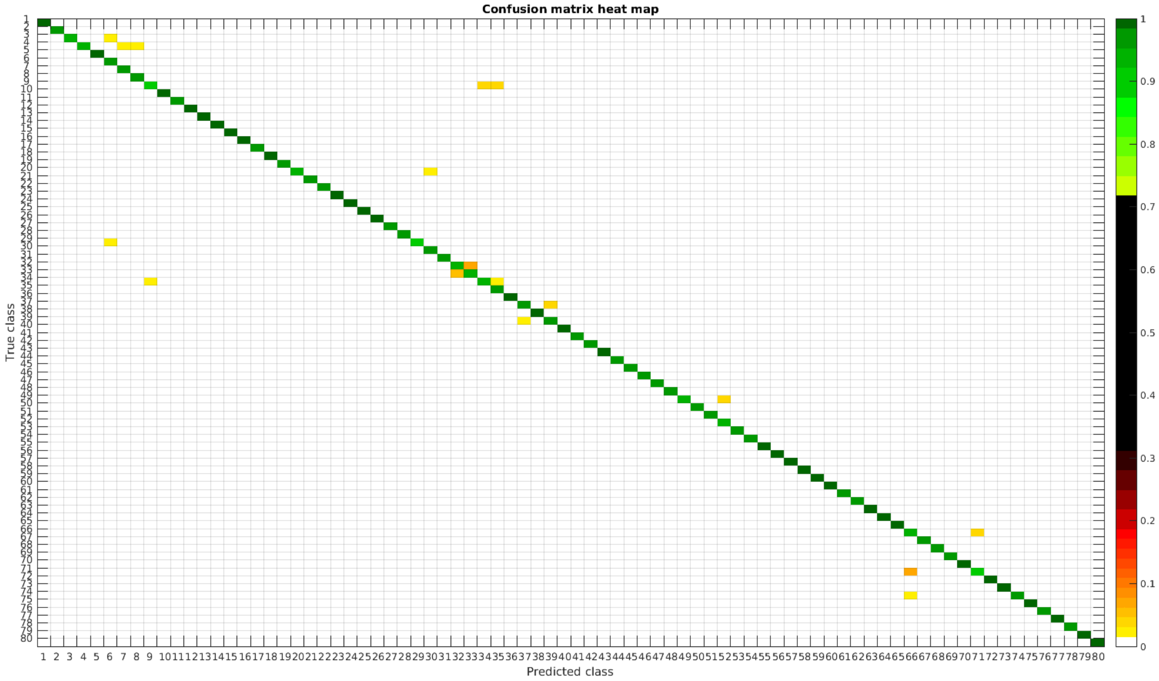

Figure 14. Confusion matrix heat map for the normalized dataset with 700 samples per class.

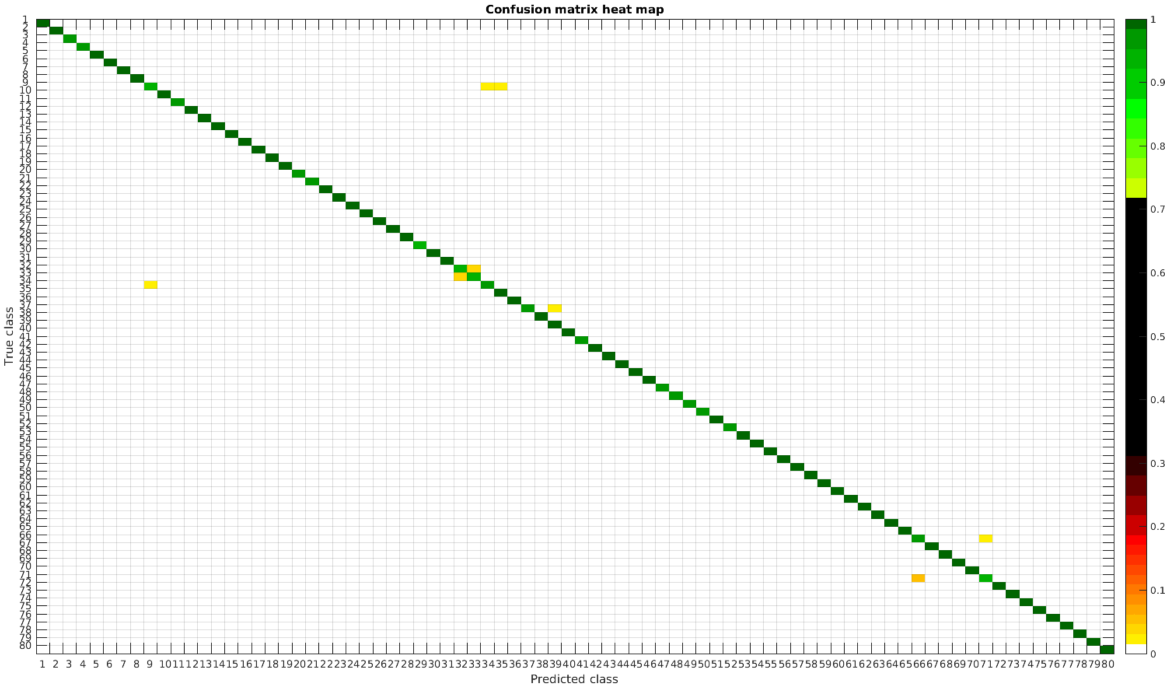

Figure 15. Confusion matrix heat map for the normalized dataset with 1000 samples per class.

In this dataset, apart from some pairs of species that are usually confused, there are some of them which are confused with more than 2, 3 or 4 species equally. Moreover, the number of misclassified classes is higher than the previous experiments when the number of samples per species is reduced. However this is quickly reduced when the number of samples per class is increased to 1000, reaching then similar accuracy values. Table 6 shows these results with the normalized database.

Table 6. Deep Learning experiments with the normalized database.

Dataset	Samples per Class	Mean Accuracy (%)	Standard Deviation
Normalized	300	93.23	0.26
Normalized	700	97.55	0.12
Normalized	1000	98.84	0.15

The following list stated some species that are misclassified and the respective species with whom they are confused:

- *Encyonema reichardtii* (29): *Achnanthidium atomoides* (2), *Achnanthidium caravelense* (3), *Achnanthidium eutrophilum* (6), *Gomphonema minutum* (52).
- *Achnanthidium rivulare* (9): *Achnanthes subhudsonis* (1), *Achnanthidium atomoides* (2), *Achnanthidium eutrophilum* (6), *Eolimna minima* (34), *Eolimna rhombelliptica* (35).
- *Nitzschia fossilis* (71): *Nitzschia amphibia* (66), *Nitzschia tropica* (74).

Even though the images are slightly different compared to the previous datasets, the classes that are more difficult to classify are similar. Finally, when the number of samples per species is over 1000, only two pairs of diatoms have some perceptible error. They are:

- *Encyonema alpina* (32) with *Encyonopsis minuta* (33).
- *Nitzschia amphibia* (66) with *Nitzschia fossilis* (71).

Figures 16 and 17 show a summary of the most frequently pairs of species that are misclassified as mentioned above.

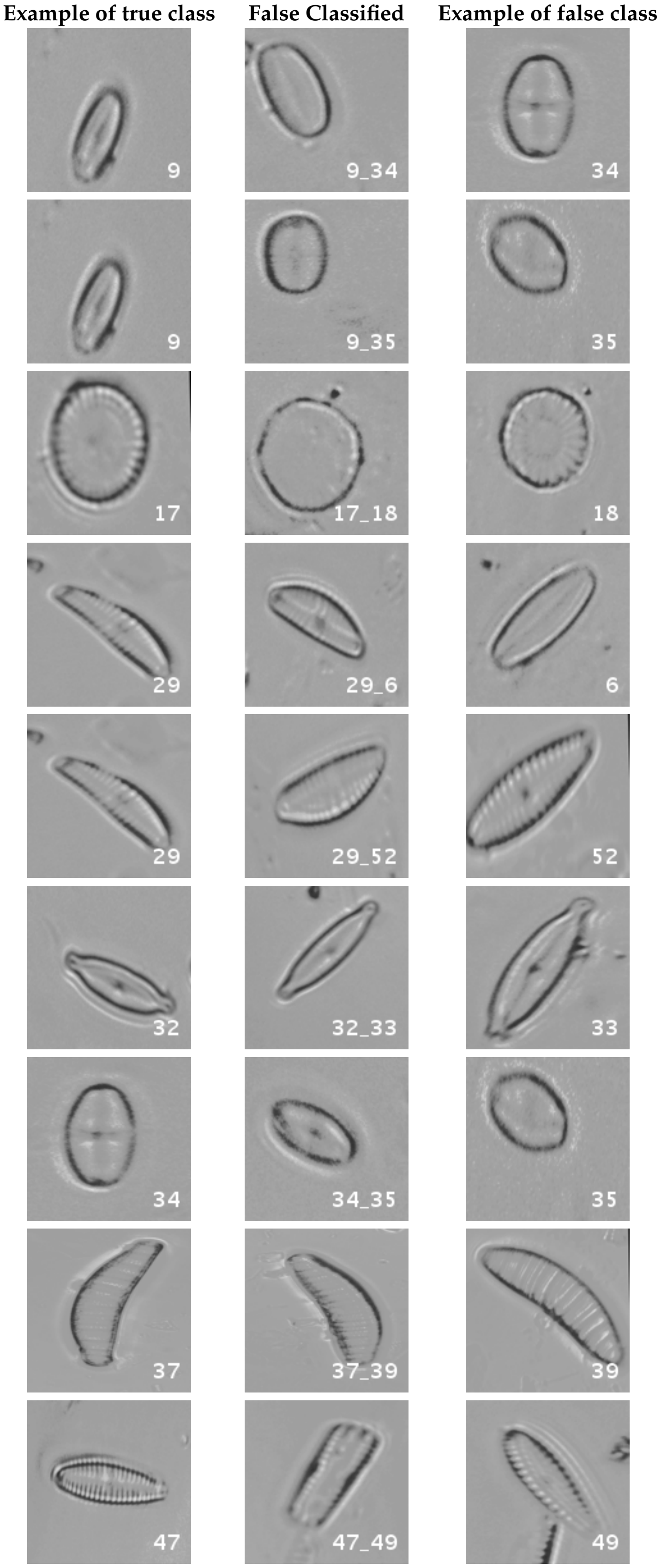

Figure 16. Normalized dataset main confusions (part 1). Each row shows an example of the true species, a missclassifed sample between two species and a sample of the second one are shown.

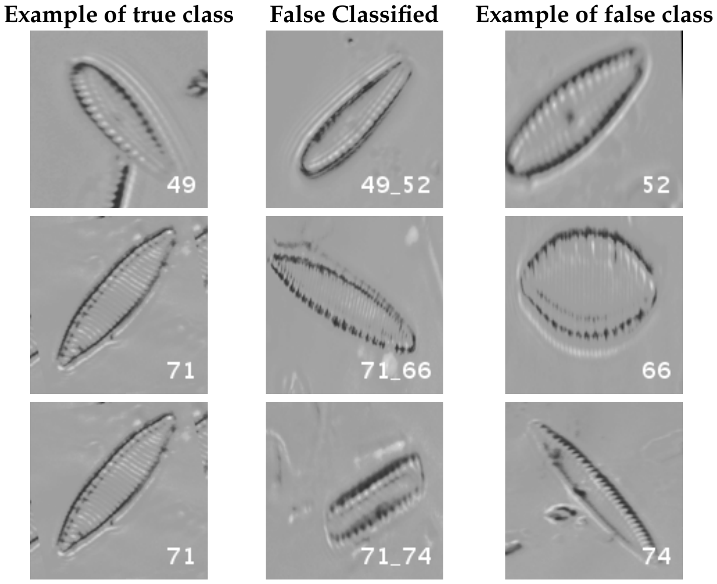

Figure 17. Normalized dataset main confusions (part 2). Each row shows an example of the true species, a missclassifed sample between two species and a sample of the second one are shown.

4.4. *Original + Normalized Dataset*

This dataset, as it was explained, is proposed to determine whether a combination of images with different preprocessing can make the model more robust. The results states that this has some impact, but the main weight in accuracy still depends heavily on the number of samples. When the balanced training process has 1000 samples per class, similar values in accuracy are obtained, and this value is even increased when 2000 samples are used.

The confusion matrices for training with 300, 700, 1000 and 2000 samples per class are presented in Figures 18–21, respectively.

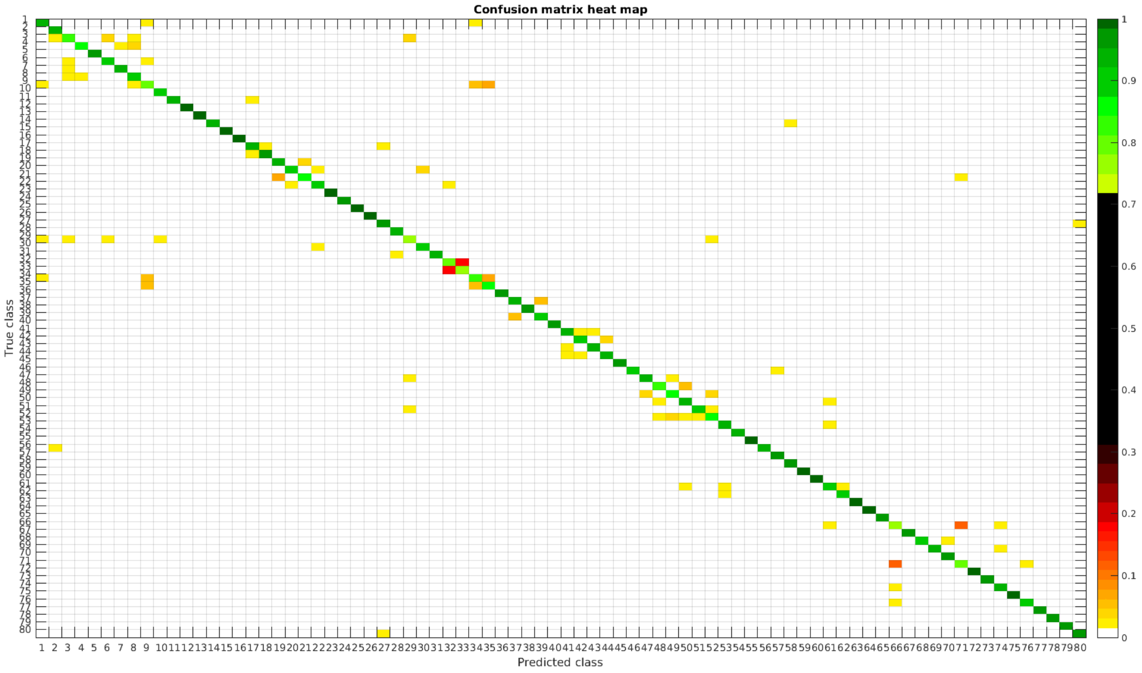

Figure 18. Confusion matrix heat map for the merged dataset with 300 samples per class.

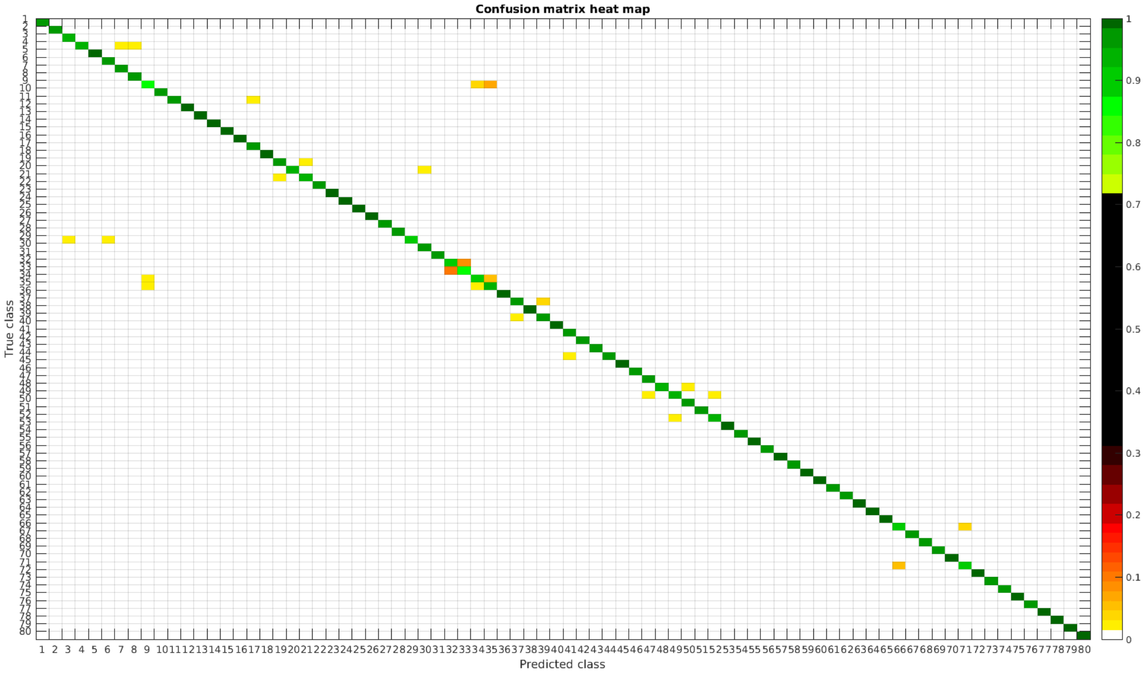

Figure 19. Confusion matrix heat map for the merged dataset with 700 samples per class.

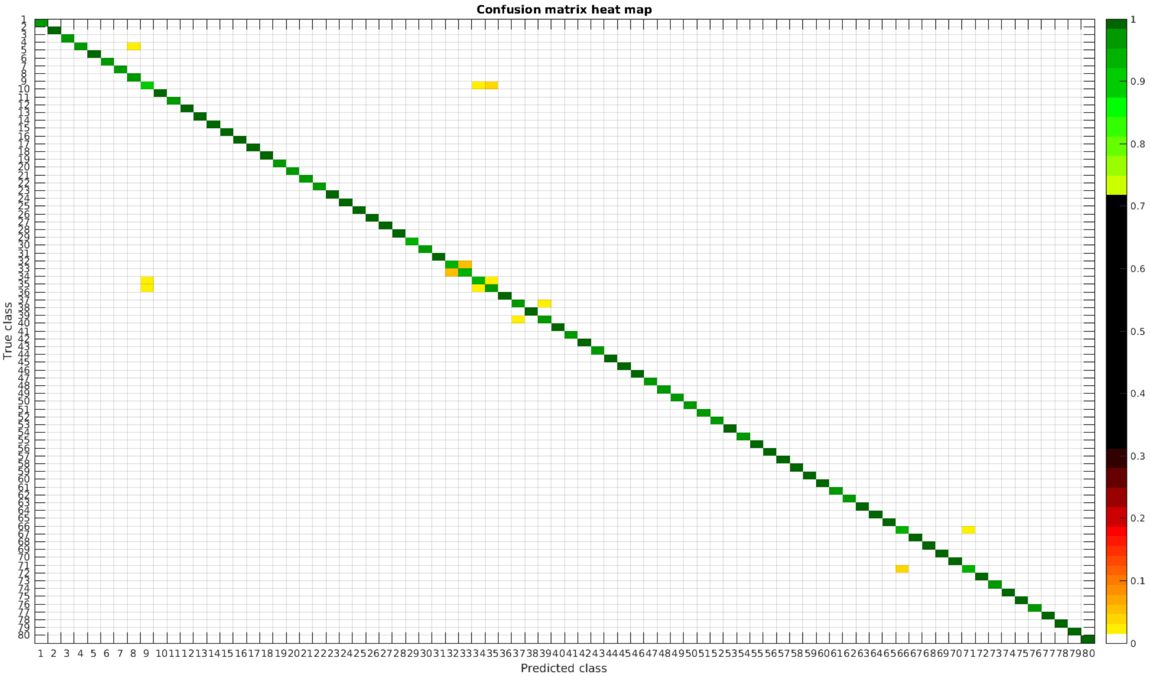

Figure 20. Confusion matrix heat map for the merged dataset with 1000 samples per class.

In terms of misclassified species, this dataset behaves in the same way as the rest, stating that even with images from different sources in terms of different processing techniques the learned model is not affected, making it quite robust in comparison with other methods.

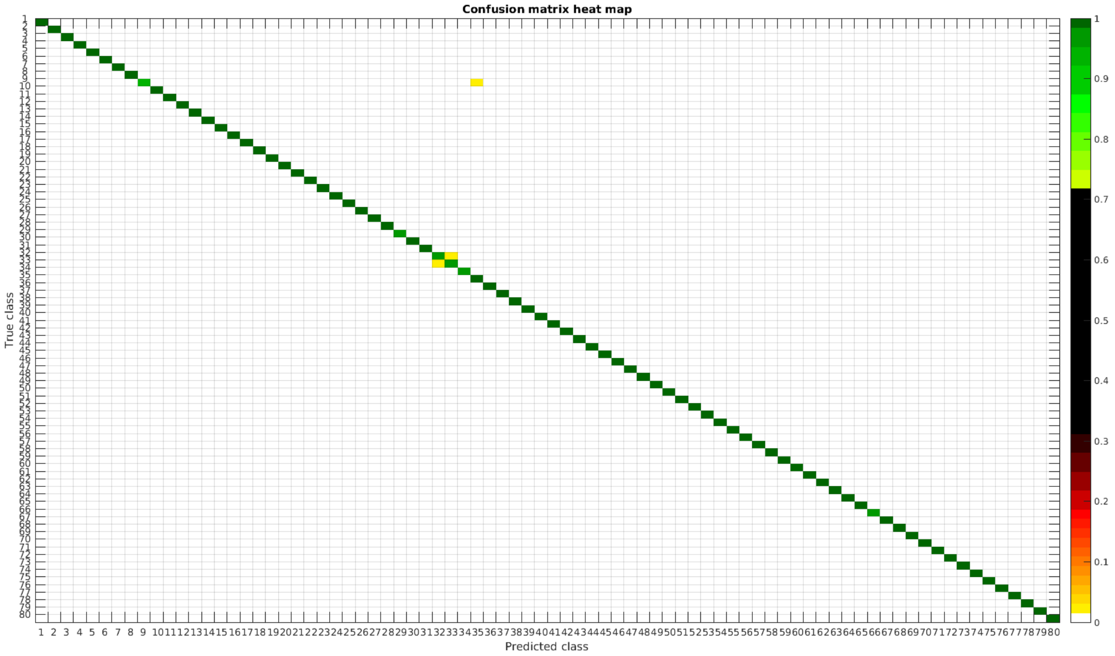

Figure 21. Confusion matrix heat map for the merged dataset with 2000 samples per class.

Table 7 shows a summary of the experiments done with this database, giving precise information about the dataset, the number of samples per class, the mean accuracy of the 10 folds from cross-validation and standard deviation. The accuracy for testing has been calculated as the percentage of labels that match between the ground truth and the classifier. Additionally, Table 8 show the top-30 species that are missclassified, with the sensitivity achieved with this model.

Table 7. Deep Learning experiments summary.

Dataset	Samples per Class	Mean Accuracy (%)	Standard Deviation
Original + Normalized	300	92.69	0.41
Original + Normalized	700	96.91	0.25
Original + Normalized	1000	98.22	0.17
Original + Normalized	2000	**99.51**	0.048

Table 8. Sensitivity of top-30 error-prone species.

Class	Sensitivity	Class	Sensitivity
Encyonopsis alpina	0.93	Navicula cryptotenella	0.99
Eolimna minima	0.96	Nitzschia fossilis	0.99
Achnanthidium rivulare	0.97	Rhoicosphenia abbreviata	0.99
Encyonema reichardtii	0.975	Achnanthes subhudsonis	0.995
Nitzschia amphibia	0.98	Achnanthidium atomoides	0.995
Achnanthidium catenatum	0.985	Achnanthidium eutrophilum	0.995
Encyonopsis minuta	0.985	Achnanthidium jackii	0.995
Gomphonema insigniforme	0.99	Cyclostephanos dubius	0.995
Achnanthidium exile	0.99	Cyclotella atomus	0.995
Amphora pediculus	0.99	Eolimna rhombelliptica	0.995
Cymbella excisa var excisa	0.99	Epithemia adnata	0.995
Gomphonema angustivalva	0.99	Fragilaria gracilis	0.995
Gomphonema micropus	0.99	Gomphonema pumilum var elegans	0.995
Gomphonema minutum	0.99	Navicula cryptotenelloides	0.995

4.5. Discussion

From the results, it is clear that accuracy is increased (and the standard deviation is decreased) when the number of training samples increases. This behavior is one of the greatest advantages of deep learning, since traditional machine learning techniques are less likely to increase their accuracy when the dataset is enlarged. It is worth noting that results improve compared to handcrafted methods when the number of samples exceeds 700 samples per class. Otherwise, the combination of several features based on morphological and textural properties may performs better with decision trees classifier than the CNN as shown in the previous study [4] (see Section 4.2).

It has been observed that, apart from the intra-dataset relation among the species that perform worse, this relation is kept inter-datasets. As a result, whichever dataset and number species for training, the species that are more difficult to be classified for CNNs are: *Encyonopsis alpina* (32), *Encyonopsis minuta* (33), *Epithemia adnata* (37) and *Epithemia turgida* (39).

Finally, when convolutional neural networks are applied, it is suitable to show how the filters that contain the learned features look like, as well as the activations that are produced with a given example.

The learned features of a CNN model are stored in the weights of its layers, being the convolutions the most significant ones. The illustration will be limited to convolution 1 and convolution 2 layers, as they are the most significant ones to be visualized. Figure 22 shows the learned filters in the convolution layer 1 of AlexNet. Attending the layer size, there are a total of 96 different filters (as it is observed in the matrix of patches), with 11×11 pixels size each. As a result, when a sample is fed throughout this layer, these filters are applied directly over the input image and each of them produce a different result, as shown in the second column of Table 9. Figure 23 shows a visualization of the weights in convolution layer 2. The structure of the layer is more complex (and so on happens when we go deeper in CNN layers). This layer has filters of 48×48 channels with 5×5 pixels size each. In the image, each of these channels is shown in a single patch. This layer has a total of 256 filters, so this is the number of output patches that are obtained when these filters are applied over the results of the previous layers, as it is observed in the third column of Table 9.

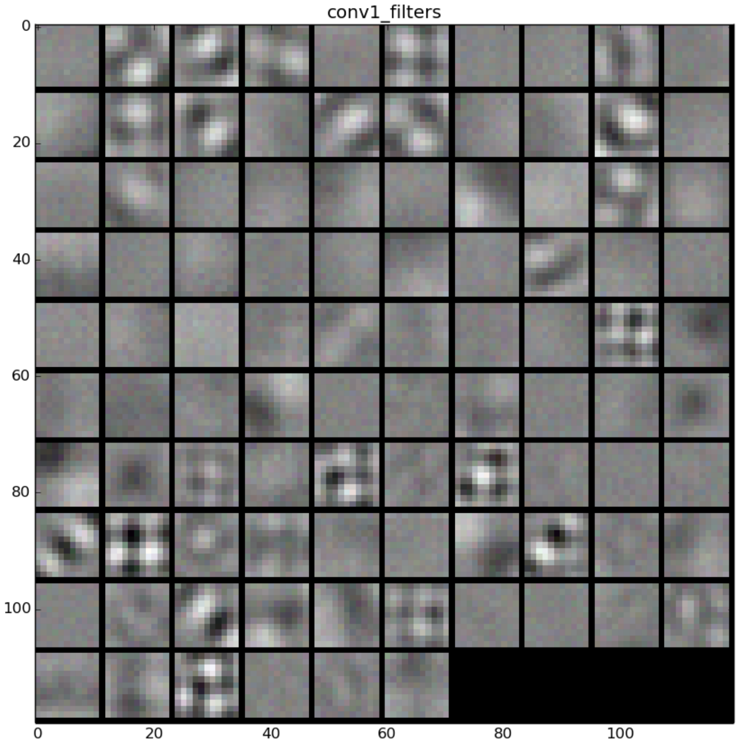

Figure 22. Filters learned in convolution layer 1.

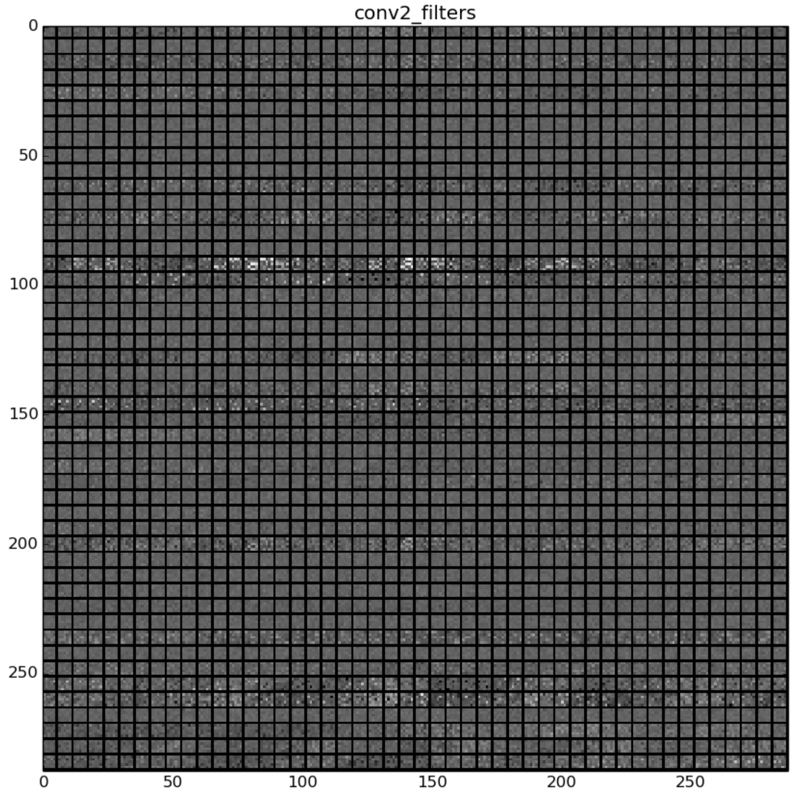

Figure 23. Filters learned in convolution layer 2.

As mentioned before, Table 9 shows two examples of diatoms from *Diatoma mesodon* and *Cyclostephanos dubius* respectively, and their corresponding activations for convolution 1 and convolution 2 layers.

Table 9. Examples of activations in the first two convolution layers in neural network. Each row shows an example of the classified diatom and the corresponding activations.

Diatom Sample	Convolution 1 Activations	Convolution 2 Activations
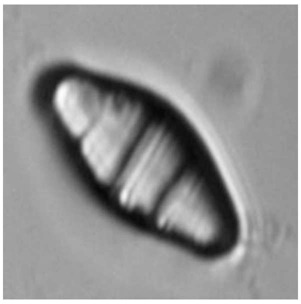	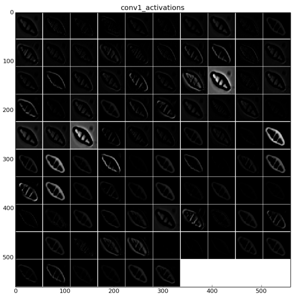	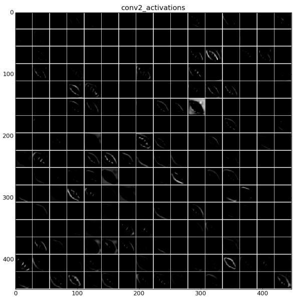
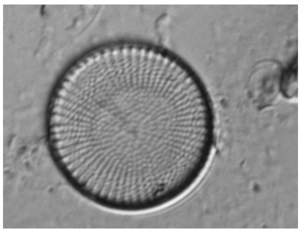	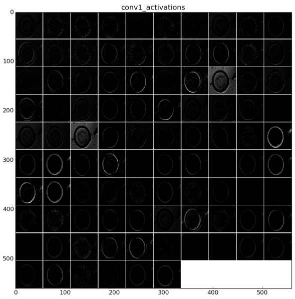	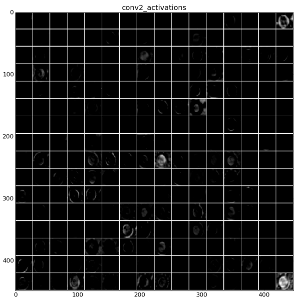

5. Conclusions

In this paper, the whole workflow of an image classification process with CNN has been covered: from dataset building, classification and results interpretation. The application of CNN to the problem of diatom classification has shown up some interesting conclusions, such as its invariance to image from different processing techniques. Hence, regarding the hypothesis that was stated about the influence of image contrast and illumination conditions on learning and discrimination, it has been proven that the results are similar regardless of the database used. Moreover, the species with larger error are usually the same. The misclassified sample is usually produced because of the presence of different views, "valve view" and "girdle view" for the same diatom type.

As far as the authors know, this is the first time that CNN has been applied to diatom classification. The applied methodology shows that the classification of large numbers of diatom species can be tackled with CNN always assuming that a large database can be provided. In our experiments with 2000 samples per class, i.e., 160,000 samples in total, an overall accuracy of 99.51% was obtained. Since CNN models take advantage from GPU computing for training but for testing too, the running time overcomes other methods, being able to process ten thousand of images in around a minute, as stated in Section 3.3.

Regarding future work, a step further would be to achieve not only classification but detection too. This way, the method would be available to determine the diatom position and species over a Whole Slide Image (WSI), so, this way, labeling and a biologist expert would not be necessary except for checking and application purposes. This can be achieved for example, using Region-based Convolutional Neural Networks (R-CNNs), or, by applying sliding windows over the image, classifying individual patches with a previously trained CNN.

Acknowledgments: The authors acknowledge financial support of the Spanish Government under the Aqualitas-retos project (Ref. CTM2014-51907-C2-2-R-MINECO) http://aqualitas-retos.es/en/.

Author Contributions: Anibal Pedraza: designed and performed the experiments. He also wrote the paper in collaboration with the rest of authors. Gloria Bueno: designed and conceived the experiments. She performs all the experiments to provide the database of segmented and normalized diatoms. She also wrote part of the paper and gave a final revision. She supervised the research and is the corresponding author. Oscar Deniz: designed and conceived the experiments. He also revised the manuscript, and supervised the research. Gabriel Cristóbal: supervised the research. Saúl Blanco: performed the data acquisition and annotation of the original database. María Borrego-Ramos: performed the data acquisition.

Conflicts of Interest: The authors declare no conflict of interest.

References

1. The European Parliament and the Council of the European Union. *Directive 2000/60/EC. Establishing a Framework for Community Action in the Field of Water Policy*; Official Journal of the European Community: Maastricht, the Netherlands, 2000.
2. Blanco, S.; Becares, E. Are biotic indices sensitive to river toxicants? A comparison of metrics based on diatoms and macro-invertebrates. *Chemosphere* **2010**, *79*, 18–25.
3. Smol, J.; Stoermer, E. *The Diatoms: Applications for the Environmental and Earth Sciences*; Cambridge University Press: Cambridge, UK, 2010.
4. Bueno, G.; Deniz, O.; Pedraza, A.; Salido, J.; Cristobal, G.; Saul, B. Automated Diatom Classification (Part A): Handcrafted feature approaches. *Appl. Sci.* **2017**, in press.
5. Dimitrovski, I.; Kocev, D.; Loskovska, S.; Dzeroski, S. Hierarchical classification of diatom images using ensembles of predictive clustering trees. *Ecol. Inform.* **2012**, *7*, 19–29.
6. Krizhevsky, A.; Sutskever, I.; Hinton, G. Imagenet classification with deep convolutional neural networks. In *Advances in Neural Information Processing Systems*; Neural Information Processing Systems Foundation, Inc.: La Jolla, CA, USA, 2012; pp. 1097–1105.
7. Szegedy, C.; Liu, W.; Jia, Y.; Sermanet, P.; Reed, S.; Anguelov, D.; Erhan, D.; Vanhoucke, V.; Rabinovich, A. Going deeper with convolutions. In Proceedings of the IEEE Conference on Computer Vision and Pattern Recognition, Boston, MA, USA, 7–12 June 2015; pp. 1–9.

8. Du Buf, H.; Bayer, M. *Automatic Diatom Identification*; Series in Machine Perception and Artificial Intelligence; World Scientific Publishing Co.: Munich, Germany, 2002.
9. Pappas, J.; Stoermer, E. Legendre shape descriptors and shape group determination of specimens in the Cymbella cistula species complex. *Phycologia* **2003**, *42*, 90–97.
10. Lai, Q.T.; Lee, K.C.; Tang, A.H.; Wong, K.K.; So, H.K.; Tsia, K.K. High-throughput time-stretch imaging flow cytometry for multi-class classification of phytoplankton. *Opt. Express* **2016**, *24*, 28170–28184.
11. Gonzalez, R.; Woods, R. *Digital Image Processing*; Pearson Prentice Hall: Upper Saddle River, NJ, USA, 2008.
12. Duchi, J.; Hazan, E.; Singer, Y. Adaptive subgradient methods for online learning and stochastic optimization. *J. Mach. Learn. Res.* **2011**, *12*, 2121–2159.
13. Nesterov, Y. *Gradient Methods for Minimizing Composite Objective Function*; Technical Report; University College London: London, UK, 2007.
14. Fawcett, T. An introduction to ROC analysis. *Pattern Recognit. Lett.* **2006**, *27*, 861–874.